Design and Optimization of One Special Microperforated Plate-Labyrinth Coupled Structure (MPPS-LS): From the View of Numerical Simulation

Zhiyuan Zhu, Lifeng Ma and Chunxiao Li

School of Mechanical and Automotive Engineering, Shanghai University of Engineering Science, Shanghai, 201620, China. E-mail: ma.lifeng-scu@foxmail.com

Xiaolong Xie

Shenda (Shanghai) Technology Co., Ltd., Shanghai, 201814, China.

Jiajia Hu

School of Mechanical and Automotive Engineering, Shanghai University of Engineering Science, Shanghai, 201620, China.

(Received 8 January 2024; accepted 16 March 2024)

Controlling large-wavelength acoustic waves via small-size structures is an important direction for the field of noise control. Since porous acoustic material can only absorb low-frequency sound waves when their thickness is approximately one-fourth of the wavelength, such acoustic material is not effective when controlling the large-wavelength acoustic waves with small-size structures. Therefore, the resonant acoustic material has been usually chosen to absorb low-frequency sound waves instead. As a typical resonant acoustic material, microperforated plate structures (MPPS), need one large cavity with low space utilization to absorb the low-frequency acoustic waves. The microperforated plate-labyrinth coupled structure (MPPS-LS) has been proposed with the goal of improving low-frequency sound absorption ability, which is consisted of a MPPS and three separated second-order LS coupled together. The mathematical model has been established using the acousto-electric analogy method and transfer matrix method to examine the impact of the structural parameters of each part on the acoustic characteristics. According to this study, the coupled structure is compact in size and has a good low and medium-frequency acoustic absorption effect, combining low and medium-frequency acoustic absorption characteristics of both the MPPS and LS. The sound absorption of the structure after optimized design is testing using impedance tube.

1. INTRODUCTION

How to efficiently reduce noise and vibration has been an urgent problem in the field of noise vibration and harshness (NVH). Generally, the induced vibration has been attenuated via highly elastic material. There exist two main methods of noise suppression: sound absorption and sound insulation. Soundproofing material could effectively impede the transmission of sound, but the attenuation of sound energy is not very significant in this process. On the other hand, sound-absorbing material could convert the incident sound energy on their surface into thermal energy dissipation, thereby achieving the effect of reducing noise. In terms of sound absorption, scholars usually use porous material to attenuate medium and high frequency noise, and resonant material to attenuate medium and low frequency noise.[1–8]

The microperforated plate structure (MPPS) consists of a layer of plates with several millimeter sized holes and a cavity, which is primarily associated with the frequency of absorption peak, behind the plate. The theoretical system of sound absorption by microperforated panels was proposed by Maa in the 1970s. This simple structure has good acoustic absorption performance and is a typical resonant sound absorption structure. However, the MPPS mainly absorbs medium and high frequency noise and its absorption effectiveness on low frequency noise is poor.[9,10] Subsequently, academician Maa had proposed a double-layer MPPS. The double-layer MPPS has improved the maximum sound absorption coefficient and effective bandwidth, compared to previous single-layer MPPS.[11] However, it doesn't significantly improve the ability of low-frequency sound absorption. Consequently, certain academics have chosen to adjust the layer quantity of the MPPS to improve the sound absorption capabilities of the framework designed for absorbing sound.[12–15] Besides, some scholars have optimized multilayer MPPS in the low frequency region: Ruiz et al applied intelligent optimization algorithms to gain the parameters of microperforated panels.[16–20] Pei designs multilayer microperforated panel sound absorption structures through deep learning. This method links the multi-layer MPPS structure with a mathematical model through machine learning, resulting in a four-layer MPPS design with improved sound absorption performance.[21] These techniques expand the sound absorption bandwidth but lead to large cavity sizes and low space utilization rates when designing for low-frequency acoustic waves. Therefore, some scholars have proposed one labyrinth structure (LS) based on spatial folding.

The LS have been proposed by Li et al.[22] It could refract sound waves inside the sound absorbing structure through the winding and folding of internal channels, which have resulted in increasing the channel length of the sound wave propagation process, thereby improving the space utilization rate of hollow space behind the resonance structure plate. According to subsequent research, the LS has good sound absorption properties in the low frequency region.[23–26] However, its application has still been limited to a certain extent due to the relatively narrow sound absorption frequency of the first order LS. Therefore, Liu and Tang proposed one second-order LS.[27,28] Under the same size, the second order LS has more sound absorption peaks under medium and low frequency. In the meantime, the second-order LS exhibits a higher sound absorption coefficient at the initial sound absorption peak compared to the first-order LS. Furthermore, with the aim of enhancing the sound absorption bandwidth of LS, several scholars have paralleled multiple LS to obtain composite structures with multiple absorption peaks.[29,30]

Based on the research, MPP exhibits better sound absorption effectiveness at high frequencies, while LS exhibits heightened ability in absorbing low-frequency sounds. Taking advantage of the fact that these two sound absorption structures could retain their respective sound absorption characteristics after being coupled, this research has proposed a novel sound absorption structure called microperforated plate-labyrinth coupled structure (MPPS-LS), which have comprised by a MPP and three second-order LS. The mathematical model of this composite structure has been established via both the acoustic-electric analogy method and the transfer matrix method.[31–35] This designed structure has been optimized using genetic algorithms to enhance its mid and low-frequency sound absorption performance.[36–40]

2. METHODS AND THEORY

2.1. Microperforated Plate Structure

The MPPS consists of a perforated cover plate with several holes, each with a diameter of less than 1 mm, arranged in a square pattern, and a cavity located behind the plate. Illustrated in Fig. 1 (a), its operational concept is analogous to that of a Helmholtz resonator. As depicted in Fig. 1 (b), as the acoustic frequency nears the resonance of the Helmholtz resonator, the resonance generated by the cavity will be excited. At this time the thermal viscous dissipation leads to a significantly decrease in acoustic energy. The schematic of equivalent circuits of MPPS could be explained by Fig. 1 (c). M_a is the acoustic quality of the micropore, R_a represents the micropore acoustic resistance, and Z_D represents the cavity acoustic impedance.

Acoustic impedance of microperforated plate:

$$Z = \frac{32\rho\nu t}{\sigma d^2}\left(\sqrt{1+\frac{x^2}{32}}+\frac{\sqrt{2}xd}{8}\right)+ j\omega\rho t\left(1+\frac{1}{\sqrt{9+\frac{x^2}{2}}}+0.85\frac{d}{t}\right). \quad (1)$$

Acoustic impedance of MPPS could be calculated as follows:

$$Z_{total} = Z_{MPP} + Z)D. \quad (2)$$

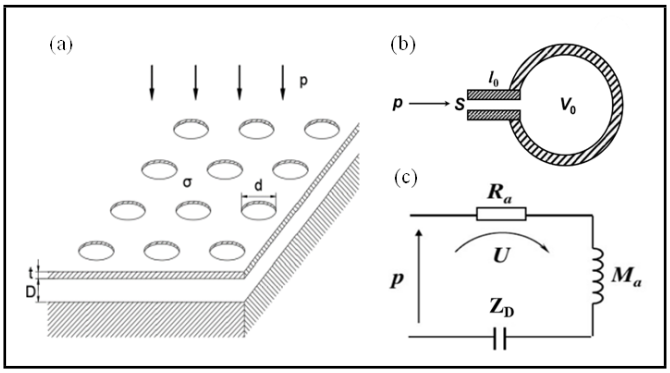

Figure 1. Microperforated panel sound absorbing structure.

The Eq. (3) could be used to obtain the acoustic impedance of the cavity behind the plate, in which the only structure parameters needed is D.

$$Z_D = -j\rho c \times \cot\left(\frac{\omega D}{c}\right). \quad (3)$$

After normalizing the acoustic impedance of MPPS using the air characteristic impedance, the acoustic impedance ratio of the microperforated plate sound absorbing could be obtained as follows:

$$Z_{total} = \frac{Z_{total}}{\rho c} = r + j\omega m - \frac{j\rho c \times \cot(\omega D/C)}{\rho c}. \quad (4)$$

The angular frequency of the sound is represented by ω, and the viscosity factor of the sound wave is represented by ν, and $\nu = 1.78910 - 5$ kg/ms, ρ stands for the density of air, $\rho = 1.21$ kg/m^3, c represents the speed of sound propagation in air, $c = 340$ m/s, d stands for the micro hole diameter, while σ represents the thin plate's perforation ratio, t stands for the thickness of the thin plate, while D represents the depth of the cavity, r is the relative sound resistivity and m is the relative sound quality, these two parameters could be obtained using Eqs. (5) and (6).

$$Z = \frac{32\rho\nu t}{\sigma d^2}\left(\sqrt{1+\frac{x^2}{32}}+\frac{\sqrt{2}xd}{8}\right); \quad (5)$$

$$m = \frac{t}{\sigma c}\left(1+\frac{1}{\sqrt{9+\frac{x^2}{g}}}+0.85\frac{d}{t}\right). \quad (6)$$

The sound absorption coefficient of the microperforated plate structure is:

$$\alpha = 1 - \left|\frac{Z_{total-1}}{Z_{total+1}}\right|^2. \quad (7)$$

When using relative sound resistivity and relative sound quality, the sound absorption coefficient could be calculated by:

$$\alpha = \frac{4r}{(1-r)^2 + (\omega m - \cot(\omega D/c)^2)}. \quad (8)$$

2.2. Labyrinth Acoustic Structure

2.2.1. First order LS

Figure 2 (a) displays the structural diagram of the LS of primary order. There are two components that make up the acoustic impedance.

$$Z_a = Z_h + Z_c; \quad (9)$$

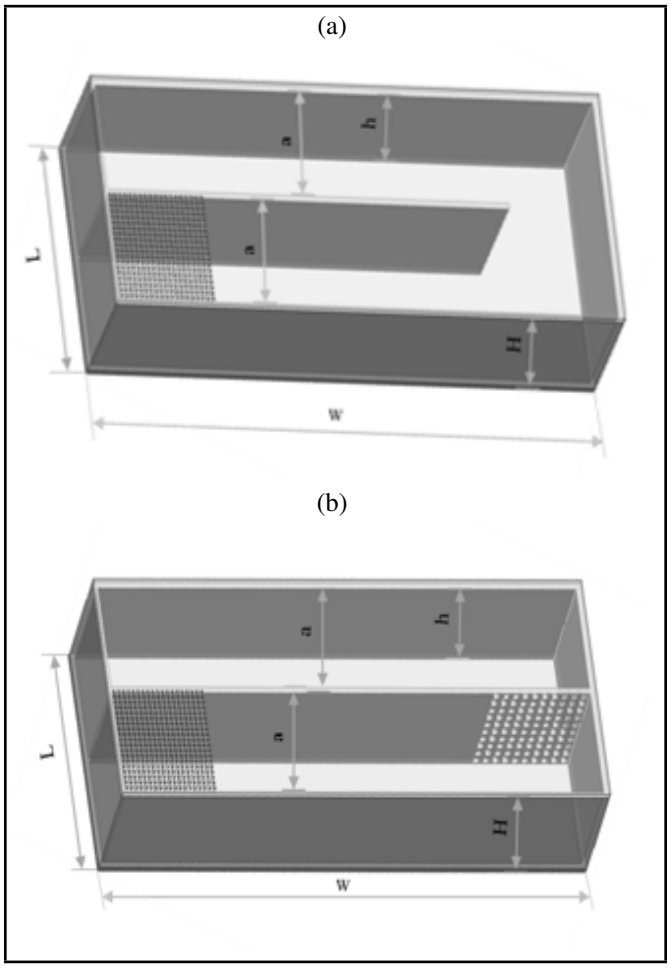

Figure 2. Schematic diagram (a) first-order LS (b) second-order LS.

where Z_a is the cumulative acoustic impedance of the structure, Z_h represents the perforated plate portion's acoustic impedance, Z_c is the acoustic impedance of the labyrinth channel portion.

The microperforated plate's acoustic impedance could be determined by means of calculation as:

$$Z_h = \frac{j\omega\rho_0}{\sigma}\left\{t_0\left[1-\frac{2B_1(\chi\sqrt{-i})}{(\chi\sqrt{-i})2B_0(\chi\sqrt{-i})}\right]^{-1}\right\}+\frac{\sqrt{2}\mu\chi}{\sigma d}; \quad (10)$$

$$\chi = d\sqrt{\rho_0\omega/4\mu}; \quad (11)$$

in which, σ is the perforation rate of the microperforated portion of the labyrinth cover plate. μ is the aerodynamic viscosity coefficient. B_0 and B_1 are the first-class Bessel functions of order 0 and 1.

The impedance Z_c of the folded cavity could be obtained from the impedance transfer formula:

$$Z_c \approx -jZ_0^e\cot(k_0^e l_0^e); \quad (12)$$

$$Z_0^e = \sqrt{\rho_0^e/C_0^e}; \quad (13)$$

$$k_0^e = \omega\sqrt{\rho_0^e C_0^e}; \quad (14)$$

where Z_0^e and k_0^e signify the impedance and transfer constant of the air contains, ρ_0^e and C_0^e are the equivalent density and equivalent volumetric compressibility of air. ρ_0^e and C_0^e could be obtained by the following formula:

$$\rho_0^e = \rho_0\frac{va^2h^2}{i4\omega}\left\{\sum_{m=0}^{\infty}\sum_{n=0}^{\infty}\left[\alpha_m^2\beta_n^2\left(\alpha_m^2+\beta_n^2+\frac{i\omega}{v}\right)\right]^{-1}\right\}^{-1}; \quad (15)$$

$$C_0^e = \frac{1}{P_0}\left\{1-\frac{i4\omega(\gamma-1)}{v'a^2h^2}\sum_{m=0}^{\infty}\sum_{n=0}^{\infty}\left[\alpha_m^2\beta_n^2\left(\alpha_m^2+\beta_n^2+\frac{i\omega\gamma}{v'}\right)\right]^{-1}\right\}; \quad (16)$$

$$\alpha_m = \frac{(m+1)\pi}{a}; \quad (17)$$

$$\beta_n = \frac{(n+1)\pi}{h}; \quad (18)$$

$$v = \frac{\mu}{\rho_0}; \quad (19)$$

$$v' = \frac{\kappa}{\rho_0 C_v}. \quad (20)$$

The intermediate calculation coefficient is represented by α_m and β_n, while the dynamic viscosity of the air is denoted as v. The thermal conductivity is κ, and C_v represents the specific constant volume heat capacity. P_0 and γ are the pressure and specific heat rate of air. T is the temperature of the environment, $T = 293.15$ K; ρ_0 is the air density, $\rho_0 = 1.21$ kg/m^2; c_0 is the sound velocity, $c_0 = 343$ m/s; P_0 is the sound pressure, $P_0 = 101325$ Pa; μ is the dynamic viscosity $\mu = 1.8\times10^{-5}$ Pa·s; κ is the thermal conductivity, $\kappa = 0.0258$ W/(m·K); C_v is the specific constant heat capacity, $C_v = 718$ J/(kg·K), γ is the specific heat rate, $\gamma = 1.4\,\text{deg}$.

The first order LS' sound absorption coefficient could be derived as:

$$\alpha = 1-\left|\frac{Z_{total}/\rho_0c_0-1}{Z_{total}/\rho_0c_0+1}\right|^2. \quad (21)$$

2.2.2. Second order LS

The second-order LS is based on the first-order LS, with another micro perforated plate built in, which is equivalent to two first-order LS arranged in series. The structural schematic is shown in Fig. 2 (b). However, due to the inability to establish an accurate relationship between the impact of the second-order labyrinth channel on the first-order LS, determining the sound absorption coefficient is not feasible by treating the two parts as a series structure using the acousto-electric analogy method. Consequently, the acoustoelectric analogy method must be used to obtain the second-order LS' sound absorption coefficient.

It could be obtained by the equivalent circuit above that:

$$Ztotal = Z_{H1}/\nu + \frac{Z_{c1}*(Z_{H2}+Z_{c2})}{Z_{c1}+\nu*(Z_{H2}+Z_{c2})}. \quad (22)$$

Formula (22) includes Z_{H1} and Z_{H2} representing the acoustic impedances of the initial and subsequent microperforated thin plates, while Z_{C1} and Z_{C2} represent the acoustic

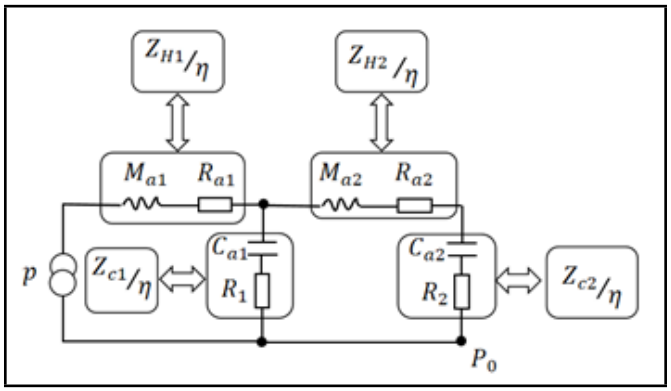

Figure 3. Equivalent circuit diagram of second-order LS.

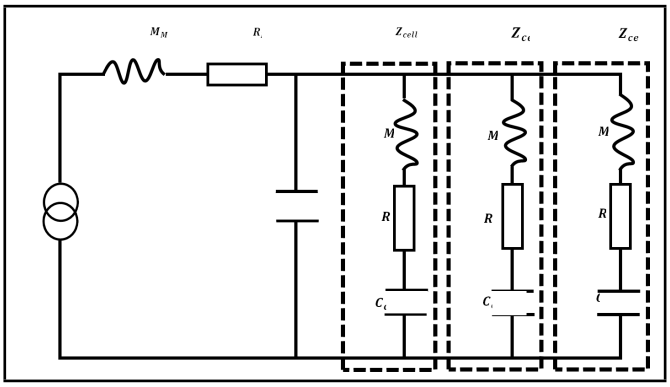

Figure 4. Acoustic and electrical analogy diagram of MPPS-LS.

impedances of the initial and subsequent labyrinth cavities. The problem could be resolved using the solution approach outlined in the initial labyrinth solution method.

The transfer matrix method could also be used to calculate the sound absorption coefficient. The impedance transfer matrices of the micropores and cavities in the i-th layer are expressed as T_{Hi} and T_{Ai}, respectively. Based on this, we could obtain the matrices of T_{Hi} and T_{Ai} below:

$$T_{Hi} = \begin{Bmatrix} 1 & Z_{Hi} \\ 0 & 1 \end{Bmatrix}; \tag{23}$$

$$T_{Ai} = \begin{Bmatrix} 1 & jZ_i^e \tan(k_i^e l_i) \\ j\tan(k_i^e l_i)/Z_i^e & 1 \end{Bmatrix}; \tag{24}$$

where the variables "k_i^e" is the effective transfer constant of the ith cavity and "Z_i^e" is the characteristic impedance of the ith cavity. Subsequently, the pressure and velocity of sound at the surface of the multi-step labyrinth are formulated as follows:

$$\begin{Bmatrix} P_1 \\ u_1 \end{Bmatrix} = T_{Hi}T_{Ai} \begin{Bmatrix} P_e \\ 0 \end{Bmatrix} = \begin{Bmatrix} T_{11} & T_{12} \\ T_{21} & T_{22} \end{Bmatrix} \begin{Bmatrix} P_e \\ 0 \end{Bmatrix}. \tag{25}$$

In the formula above, P_e is the lowest sound pressure of multiple steps, and its corresponding mass velocity is 0.

The acoustic reflection coefficient R is expressed as:

$$R = \frac{T_{11} - \rho_0 c_0 T_{21}}{T_{11} + \rho_0 c_0 T_{21}}. \tag{26}$$

The definition formula of coefficient is:

$$\alpha = 1 - |R|^2. \tag{27}$$

From the above formula, we could obtain that coefficient of the second-order LS is:

$$\alpha = \frac{4Re(\frac{Z_{Hi}}{\rho_0 c_0})}{\left[1 + Re(\frac{Z_{Hi}}{\rho_0 c_0})\right]^2 + \left[Im(\frac{Z_{Hi}}{\rho_0 c_0})\right]^2}. \tag{28}$$

2.3. Microperforated Plate-Labyrinth Coupled Structure

The absorption coefficient of the coupled structure can be determined using the acoustic-electric analogy method. The acoustic-electric analogy diagram is shown in Fig. 4. To improve the computational accuracy of the model, the transfer matrix method is used when calculating the absorption coefficient of individual second-order labyrinth structures. When calculating the absorption coefficient of the coupled structure of micro-perforated panel and labyrinth, the acoustic-electric analogy method is adopted.

Thus, the absorption coefficient of the coupled structure can be obtained:

$$Z_{total} = Z_{MPP} + \frac{C_{MPP} Z_{cell}}{C_{MPP} + Z_{cell}}; \tag{29}$$

$$Z_{cell} = \frac{Z_{cell1} Z_{cell2} Z_{cell3}}{Z_{cell1} Z_{cell2} + Z_{cell1} Z_{cell3} + Z_{cell2} Z_{cell3}}. \tag{30}$$

In the equation, Z_x represents the acoustic impedance of the x component, which can be obtained from Fig. 4.

3. NUMERICAL SIMULATION ANALYSIS

3.1. Microperforated Panel Structure

A perforated plate with $\sigma = 0.005$, $t = 1$ mm, $D = 10$ mm and $d = 0.3$ mm was used as the base to investigate the consequence of different structural parameters.

Figure 5 (a) shows as the aperture diameter experiences growth, the absorption capacity of the MPPS was enhanced in $0 - 1500$ Hz, the absorption bandwidth became narrower, and the absorption capacity at the first curve peak was enhanced. As σ increased, the absorption band of the MPPS with the absorption coefficient value exceeding 0.5 during $0 - 1500$ Hz became wider, the frequency of first peak tended to migrate to high frequency, and the absorption coefficient at its first absorption peak increased. It could be seen from Fig. 5 (c) that as the thickness of the MPPS increased, the absorption band with the absorption coefficient greater than 0.5 became narrower in $0 - 1500$ Hz. The initial absorption peak frequency shifted towards lower ranges, leading to a reduction in the absorption coefficient at that peak. It could be seen from Fig.5 (d) that the MPPS' frequency of its first absorption peak tended to lower direction as the depth of cavity behind the MPPS increases.

3.2. Labyrinth Structure

3.2.1. First order labyrinth acoustic structure

The first-order LS with $\sigma = 0.03$, $t = 1$ mm, $l0 = 80$ mm and $d = 0.3$ mm was used as the basis to investigate the effect of different structural parameters on the sound absorption capability.

The effect of structural parameters on the absorption coefficient of the first-order LS could be obtained from Fig. 6. As the perforation diameter d increased, the first absorption peak's

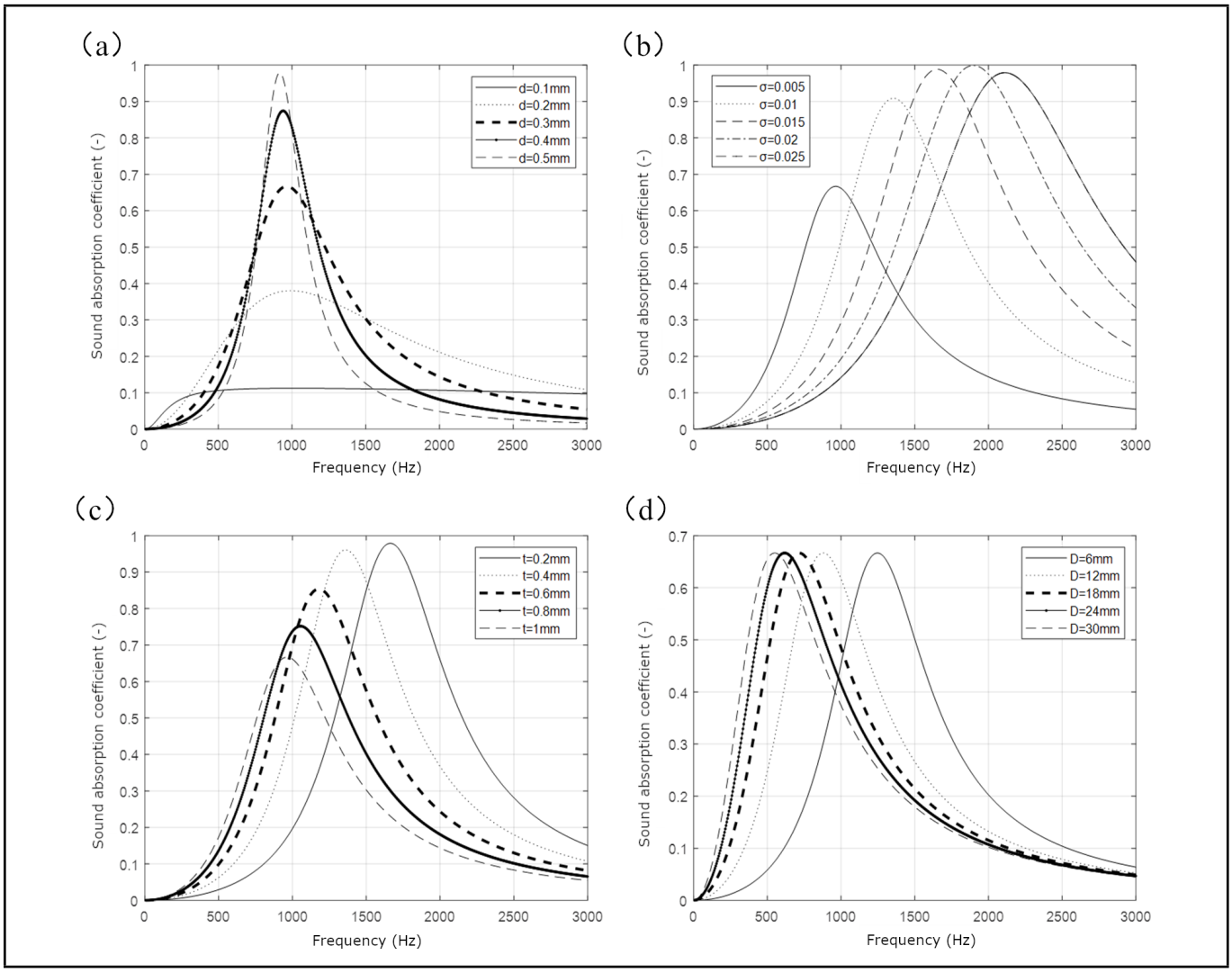

Figure 5. Influence of structural parameters on sound absorption performance of perforated panel sound absorption structure.

frequency migrated towards the lower end, resulting in an augmented absorption coefficient at that peak. With the increase of the perforation rate σ, the first absorption peak shifted towards higher frequencies, leading to an increase in the absorption coefficient. As the plate thickness t increased, the initial absorption peak shifted towards the lower frequency range, resulting in a reduction of the absorption coefficient at the peak. As the length of the labyrinth channel l_0 increased, the initial absorption peak shifted towards the lower frequency range, and the absorption coefficient at the peak remained almost the same.

As the incident area ratio ν decreased, the frequency corresponding to the first absorption peak remained almost unchanged, and the absorption coefficient corresponding to the first absorption peak decreased.

3.2.2. Second order labyrinth acoustic structure

The second-order LS with $\sigma_1 = 0.03$, $\sigma_2 = 0.03$, $t_1 = 1$ mm, $t_2 = 1$ mm, $l_1 = 40$ mm, $l_2 = 40$ mm, $d_1 = 0.3$ mm, $d_2 = 0.3$ mm, was used as the basis to examine how different structural parameters influence the sound absorption performance.

It could be concluded from Fig. 7 that as the size of the first-order labyrinth's diameter d_1 and the second-order labyrinth's diameter d_2 increased, the frequency at which the first absorption peak occurs in the acoustic structure decreased, and the absorption coefficient for that peak also increased. With the increase in the perforation rate σ_1 of the initial LS and the perforation rate σ_2 of the secondary LS, the acoustic structure's first absorption peak frequency shifts towards higher frequencies, leading to an increase in the corresponding absorption coefficient. As the thickness t_1 of the first-order LS and the thickness t_2 of the second-order LS increased, the first absorption peak frequency shifted to lower frequencies, and the absorption coefficient at the first absorption peak decreased. As the labyrinth channel length l_1 of the first-order LS and the labyrinth channel length l_2 of the second-order LS increased, it would make the first absorption peak frequency of the acoustic structure shift to lower frequencies.

As the proportion ν of the microperforated section to the total incident area rose, the frequency linked to the initial absorption peak remained relatively constant, while the absorption coefficient associated with the initial absorption peak declined, and the range of frequency ranges with absorption coefficients exceeding 0.5 became narrower.

3.3. Microperforated Panel Single Labyrinth Acoustic Structure

In the case of an acoustic frequency range of $0 - 1500$ Hz, the microperforated plate structure exhibited a single absorp-

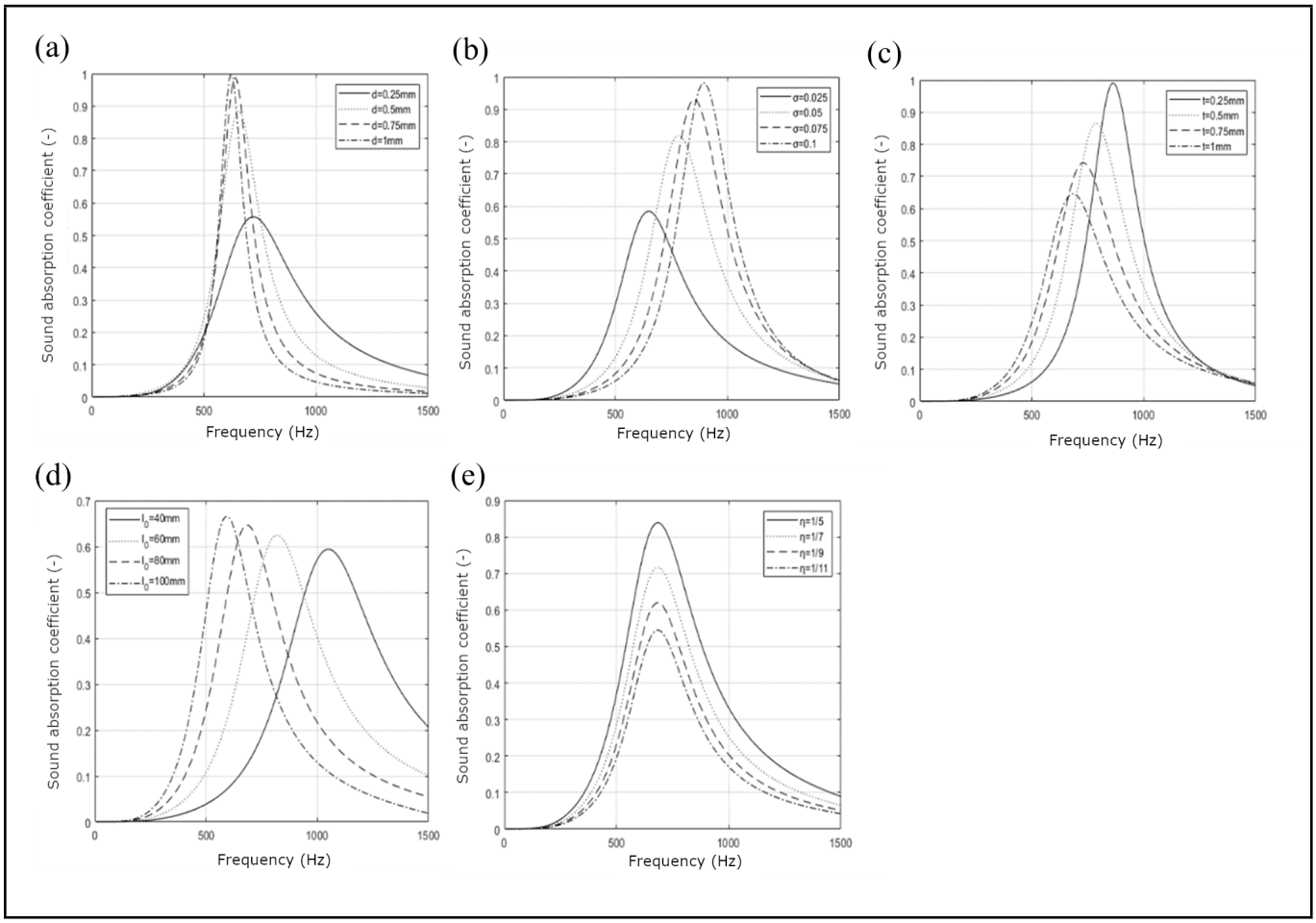

Figure 6. Influence of structural parameters on sound absorption of first-order labyrinth structure.

tion peak, whereas the LS structure showed two absorption peaks. However, the coupled structure of both displayed three absorption peaks. The absorption peak of the MPP structure's absorption coefficient curve was at 810 Hz, with a maximum absorption coefficient of 0.45; The LSAS structure had two absorption peaks at 305 Hz and 920 Hz, with absorption coefficients of 0.96 and 0.81, respectively; The MPP-LSAS structure exhibited three absorption peaks at 290 Hz, 765 Hz, and 945 Hz, with absorption coefficients of 0.97, 0.53, and 0.98, respectively. The three absorption peaks of the coupled configuration primarily aligned with the absorption peak of each coupling component, indicating that the coupled configuration expanded the absorption range of the structure. Additionally, the coupled configuration preserved the distinctive features of each coupling component. Moreover, the absorption coefficient at the peak of the coupled configuration surpassed that of the individual acoustic structure. Consequently, coupling the microperforated plate structure with the LS proves advantageous in broadening the absorption range of the coupled configuration. Additionally, by making reasonable adjustments to the parameters, the sound absorption performance of the structure could be improved further.

3.4. Microperforated Plate Labyrinth Coupled Structure

Figure 9 shows the absorption coefficient of the coupled structure and the absorption coefficients of the MPPS and the coupled LS that constitute the coupled structure at the acoustic frequency range of $0 - 3000$ Hz. The structure exhibits three absorption peaks, which are near the absorption peaks of the MPPS and the LS. The first and second absorption peaks were provided by the underlying parallel LS. The frequency of the first absorption peak was 465 Hz, with an absorption coefficient of 0.89, while the frequency of the second absorption peak was 1190 Hz, with an absorption coefficient of 0.99. The third absorption peak was provided by the upper layer MPPS, with a frequency of 2010 Hz and a maximum absorption coefficient of 0.62. Additionally, the frequencies associated with the absorption peaks of the coupled structure were lower compared to those of the individual structure. The frequency associated with the highest point of the combined structure was less than that of the highest point of the separate structure. This leads to a certain increase in the absorption coefficient.

4. STRUCTURAL OPTIMIZATION

4.1. Optimization Target

Genetic algorithm is a heuristic algorithm that generates a solution during the search process that guides the value of the subsequent iteration process towards the optimal solution. Therefore, when the algorithm iterates a certain number of times, its value is very close to the global optimal solution, thereby achieving global optimization. Increasing the weight of coefficients in the low and mid-frequency portion of the established function shifts the structure's sound absorption performance towards the low and mid-frequency direction in this

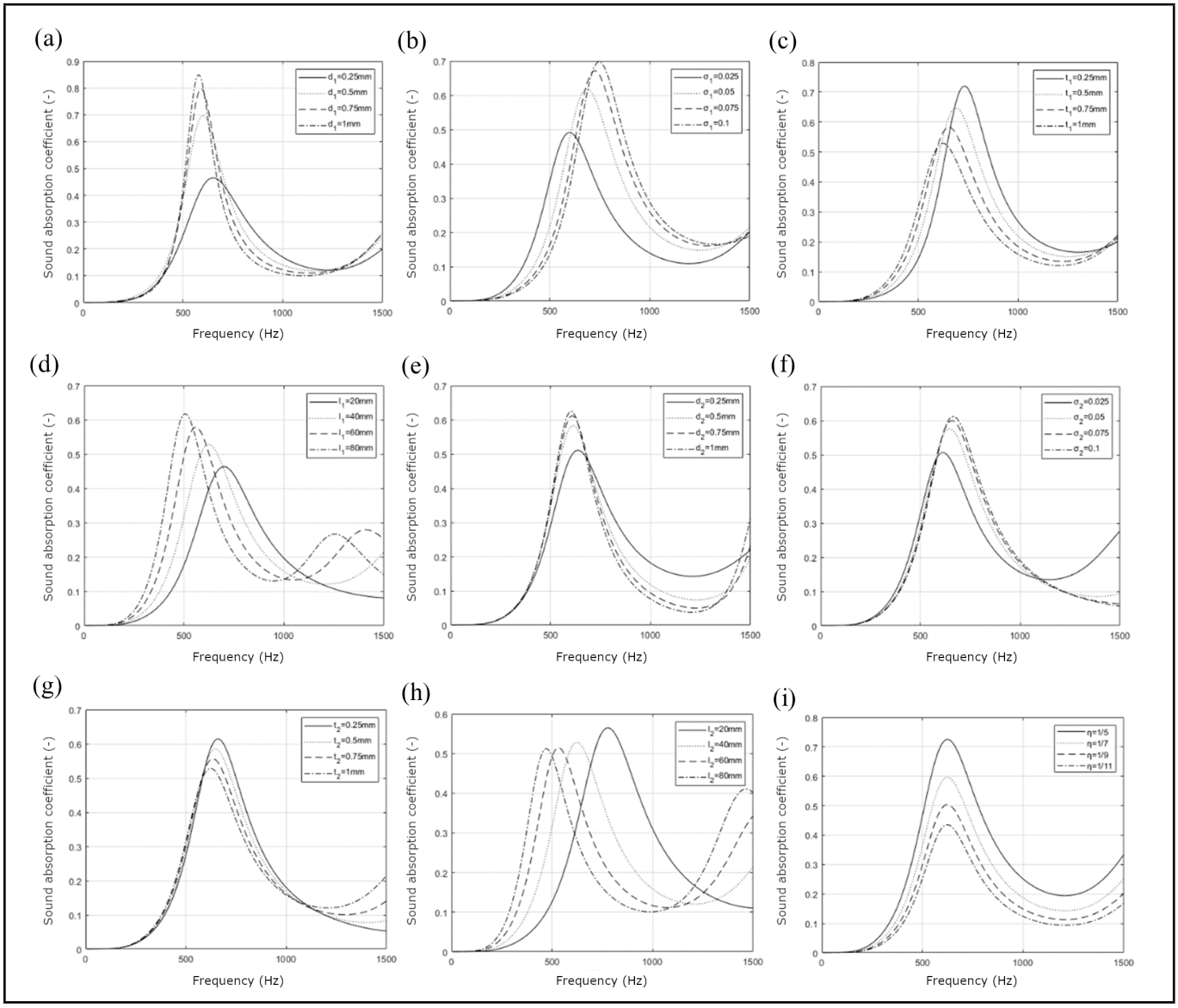

Figure 7. Structural parameters' effect on sound absorption performance of second-order LS.

research. The fitness function was set as:

$$fit = \sum_{i=1}^{300} \frac{\alpha(5i)}{5i}. \tag{31}$$

$0-1500$ Hz was divided into 300 intervals with a unit length of 5 Hz each. Here, i represented the interval number, and α represented the absorption coefficient of that interval.

4.2. Genetic Algorithm For Structural Parameters

With N set as 50 for the initial population, P_j as 0.8 for the crossover probability of chromosomes, P_b as 0.05 for the mutation probability of genes, and Gen as 200 for the genetic algebra.

4.2.1. Microperforated plate structure

Table 1 displays the value range of each parameter for the MPPS. The fitness curves for the current optimization shows that the fitness curve of single layer microperforated panels converged after 170 iterations when optimized using genetic algorithm. Currently, Tab. 1 displays the structural characteristics of microperforated panels, while Fig. 10 illustrates the curve of the sound absorption coefficient. Currently, the resonance frequency is 1052 Hz, the range of sound absorption extends to one-third of the frequency band, and the highest sound absorption factor reaches 0.98.

Table 1. Basic parameters of the recognition model.

Parameter	d/mm	σ	t/mm	l/mm
Parameter value	d=0.138	σ=0.048	t=0.735	D=60

4.2.2. Labyrinth acoustic structure

Table 2 displays the range of values for each parameter in the labyrinth acoustic structure. The fitness curve of the genetic algorithm for optimization shows when the number of iterations reaches 120, the fitness evolution curve approaches convergence by optimizing the labyrinth structure of the first order. Similarly, by optimizing the second-order LS, convergence was approached when the iterations were 100. The optimized second-order LS has a smaller objective function value than the first-order LS when converging, when the acoustic frequency was between 0 and 1500 Hz.Hence, it could be inferred

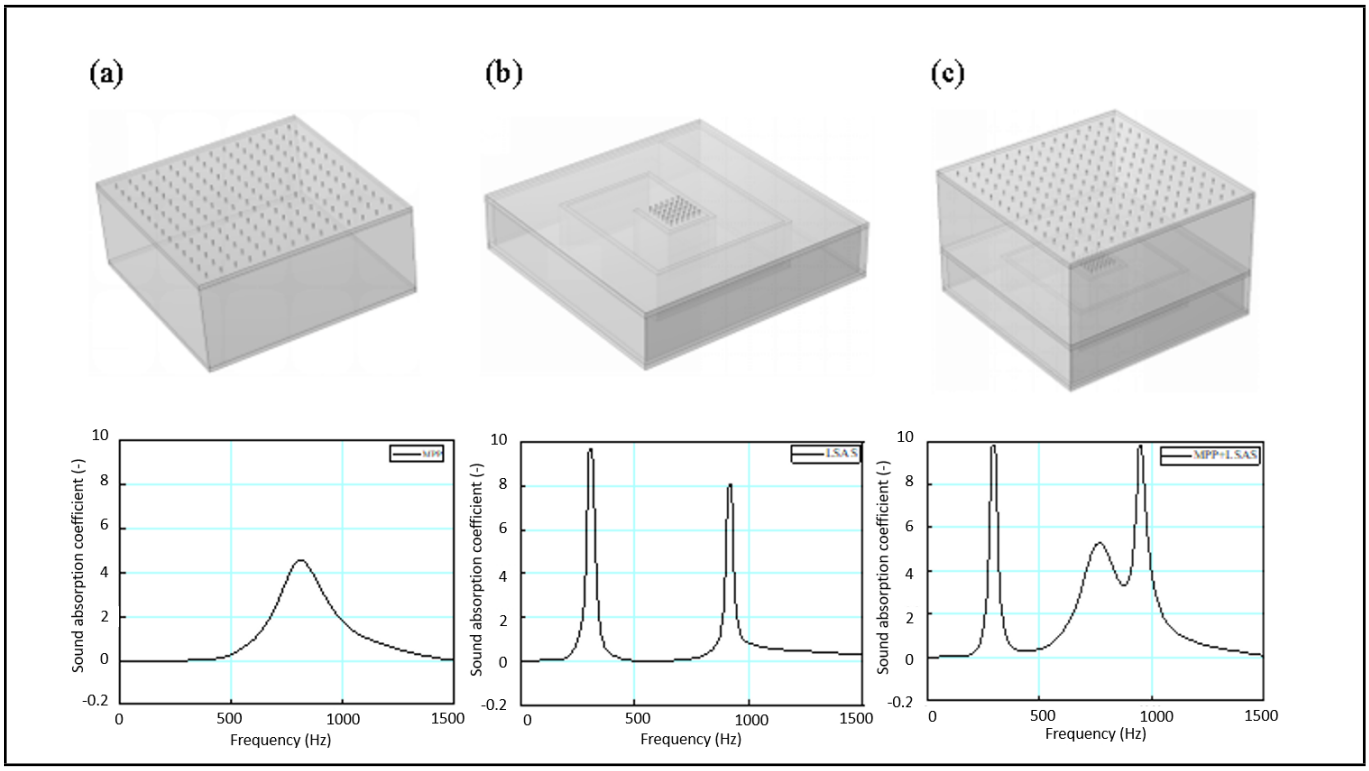

Figure 8. Schematic diagram and sound absorption coefficient (a) MPPS (b) LS (c) MPPS-LS.

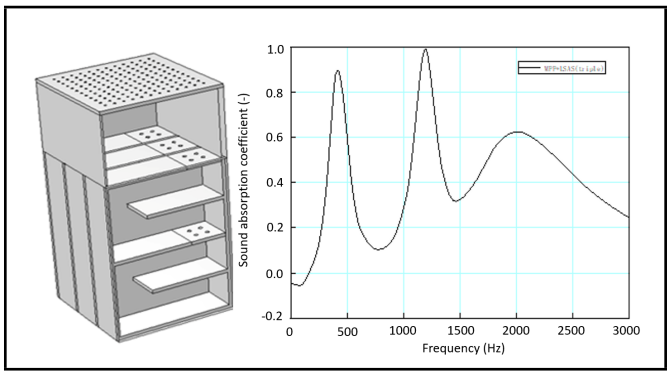

Figure 9. Schematic diagram and sound absorption coefficient of MPPS-LS.

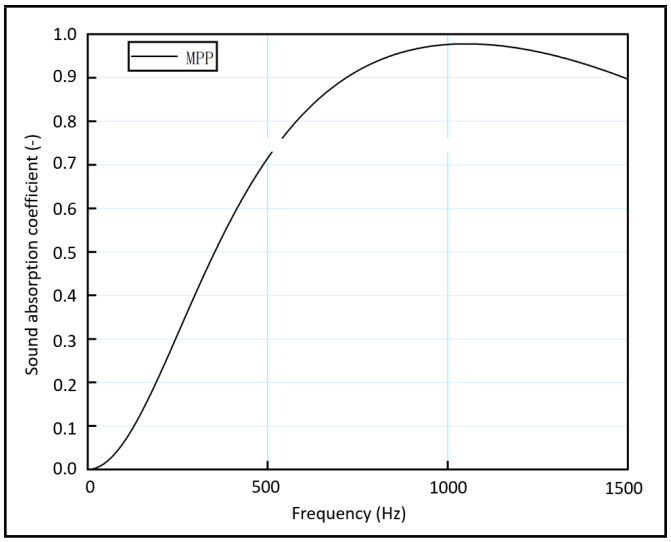

Figure 10. Sound absorption coefficient curve of optimized MPPS.

Table 2. The parameters of optimized LS.

Parameter	d/mm	σ	t/mm	l/mm
First-order LS	d=0.208	σ=0.098	t=0.912	l=80.000
Second-order LS (1)	d_1=0.902	σ_1=0.097	t_1=0.214	l_1=64.26
Second-order LS (2)	d_2=0.251	σ_2=0.005	σ_2=0.005	l_2=15.74

that the optimized second-order LS exhibits superior sound absorption capabilities compared to the optimized first-order LS within the frequency range of $0-1500$ Hz. Table 2 displays the parameters for the optimized first-order labyrinth structure and the optimized second-order labyrinth structure. Fig. 11 illustrates the curve representing the sound absorption coefficient. The optimized first-order LS clearly exhibited a peak in sound absorption at a frequency range of $0-1500$ Hz, with the peak absorption occurring at 890 Hz. Similarly, the optimized second-order LS demonstrated two sound absorption peaks within the $0-1500$ Hz frequency range, with the first and second peak absorption frequencies being 840 Hz and 1360 Hz. In comparison to the initial LS, the first peak of sound absorption shifts towards lower frequencies, expanding the frequency range of sound absorption. However, the maximum sound absorption coefficient of the peak would decrease.

4.2.3. Microperforated plate labyrinth coupled structure

Previous studies could be used to determine the range of selection for each structural parameter. The range of parameters for the MPPS part is shown in Tab. 3, and the range of parameters for the labyrinth part is shown in Tab. 3. Set the initial population of genetic algorithm $N = 50$, the crossover probability of chromosome $P_j = 0.8$, the variation probability of gene $P_b = 0.05$, the number of generations $Gen = 200$. Figure 3 shows the fitness of optimization. It could be found that the optimization process converged after approximately 80 it-

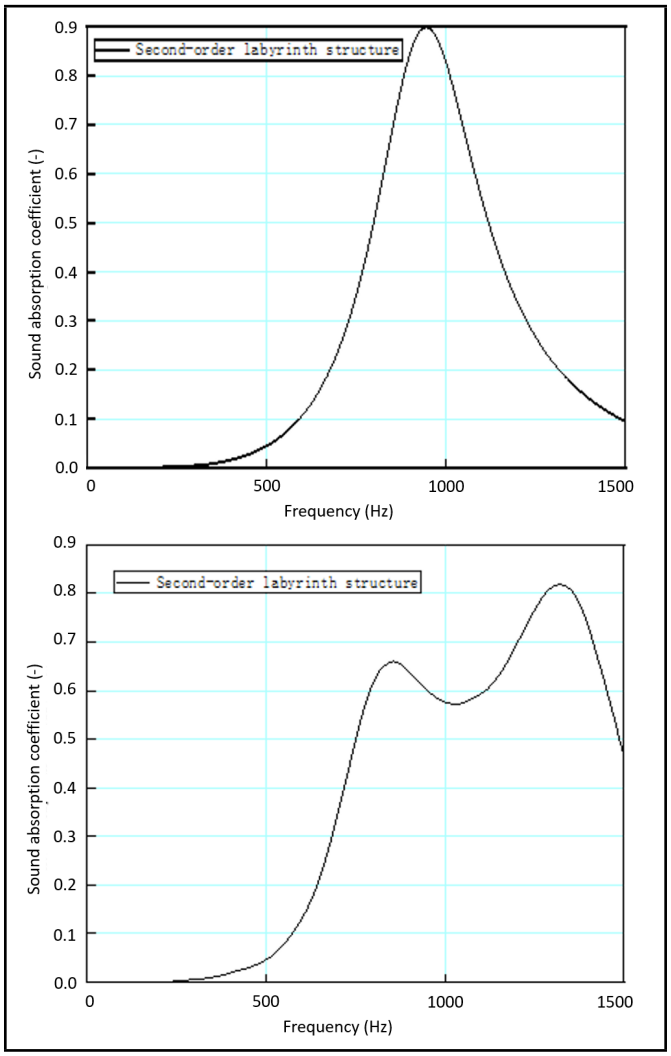

Figure 11. Sound absorption coefficient curves of optimized first and second order LS.

erations. The structural parameters of the optimized MPPS and three LS are shown in Tab. 3. Process the samples according to the structural parameters in Tab. 3. Utilize 3D printing to create the maze framework and employ laser perforation to obtain the perforated plate. The processed samples are depicted in Fig. 12 (a). The absorption coefficient curve of the coupled acoustic structure is shown in Fig. 12 (b). The finely-tuned coupled system demonstrates several absorption peaks across the $0-1500$ Hz acoustic frequency range, with absorption coefficients exceeding 0.7 for each peak. Additionally, the average absorption coefficient for the $0-1500$ Hz acoustic frequencies is greater than 0.6. As for the obtained absorption coefficient curves from the experiments, the trend and values of the first absorption peak are essentially consistent with the numerical simulation results, with the experimental absorption coefficient even higher. The second absorption peak deviates towards a lower frequency by 200 Hz compared to the theoretical values.

The experimental results for the third absorption peak are noticeably lower than expected, and the frequency has shifted towards higher frequencies. It is speculated that this discrepancy may be attributed to the upper layer microperforated panel not being installed perfectly flush with the surrounding resin, which prevents the microperforated panel from achieving optimal sound absorption performance as originally designed to match the cavity. This has resulted in an overall shift in the third absorption peak.

Table 3. Parameter values of MPPS-LS.

Parameter	d/mm		σ		t/mm		D/mm	
MPPS	0.3845		0.0065		0.5		20	
Parameter	d_1/mm	σ_1	t_1/mm	L_1/mm	d_2/mm	σ_2	t_2/mm	L_2/mm
LS-unit 1	0.8669	0.08	1	55	0.3	0.005	1	76
Parameter	d_1'/mm	σ_1'	t_1'/mm	L_1'/mm	d_2'/mm	σ_2'	t_2'/mm	L_2'/mm
LS-unit 2	0.9685	0.0833	0.5595	55	0.3	0.0104	0.503	76
Parameter	d_1"/mm	σ_1"	t_1"/mm	L_1"/mm	d_2"/mm	σ_2"	t_2"/mm	L_2"/mm
LS-unit 3	0.3509	0.09	1	98	0.3	0.0023	0.512	33

5. CONCLUSION

To address low-frequency noise, a microperforated plate labyrinth coupled structure has been proposed based on MPPS and LS. It consists of a MPPS and three second-order LS. A mathematical model of the coupling structure, MPPS-LS, is established using the acoustic-electric analogy method and the transfer matrix method first. Then, effect of all structures of each component on the sound absorption property have been explored. Finally, the sound absorption performance has been optimized by using genetic algorithms. It could be observed that the coupled structure exhibits characteristics of both the MPPS and LS, with three absorption peaks in the $0-1500$ Hz range, the numerical simulation yields three absorption peaks in the absorption coefficient curve at 480 Hz, 885 Hz, and 1260 Hz, corresponding to absorption coefficients of 0.76, 0.82, and 0.90, respectively. Through experimentation, three absorption peaks in the absorption coefficient curve are observed at 505 Hz, 725 Hz, and 1410 Hz, with corresponding absorption coefficients of 0.91, 0.89, and 0.70.

Compared to the perforated plate and LS, the coupled structure significantly improved in low frequency. Within the $0-1500$ Hz range, the structure has multiple absorption peaks, and between $360-1500$ Hz, the average sound absorption coefficient of MPPS-LS designed reaches 70 %. Finally, the sample was processed using 3D printing and laser perforation techniques. The absorption coefficient of the samples is tested using the impedance tube method.

ACKNOWLEDGEMENTS

This work was supported by the National Natural Science Foundation of China (No. 51903150 and 52172371), Program of Shanghai Academic/Technology Research Leader (No. 21XD1401100), Technical Service Platform for Noise and Vibration Evaluation and Control of New Energy Vehicles (No. 18DZ2295900) at Science and Technology Commission of Shanghai Municipality, China.

REFERENCES

[1] Tao, Y.P., Ren, M.S., Zhang, H. and Peijs. T. Recent Progress in Acoustic Materials and Noise Control Strategies – A Review. *Applied Materials Today*, **24**, 101141, (2021). https://doi.org/10.1016/j.apmt.2021.101141

[2] Ma, L.F., Yang, W. and Jiang, C. Stretchable Conductors of Multi-Walled Carbon Nanotubes (MWCNTs) Filled Thermoplastic Vulcanizate (TPV) Composites with Enhanced

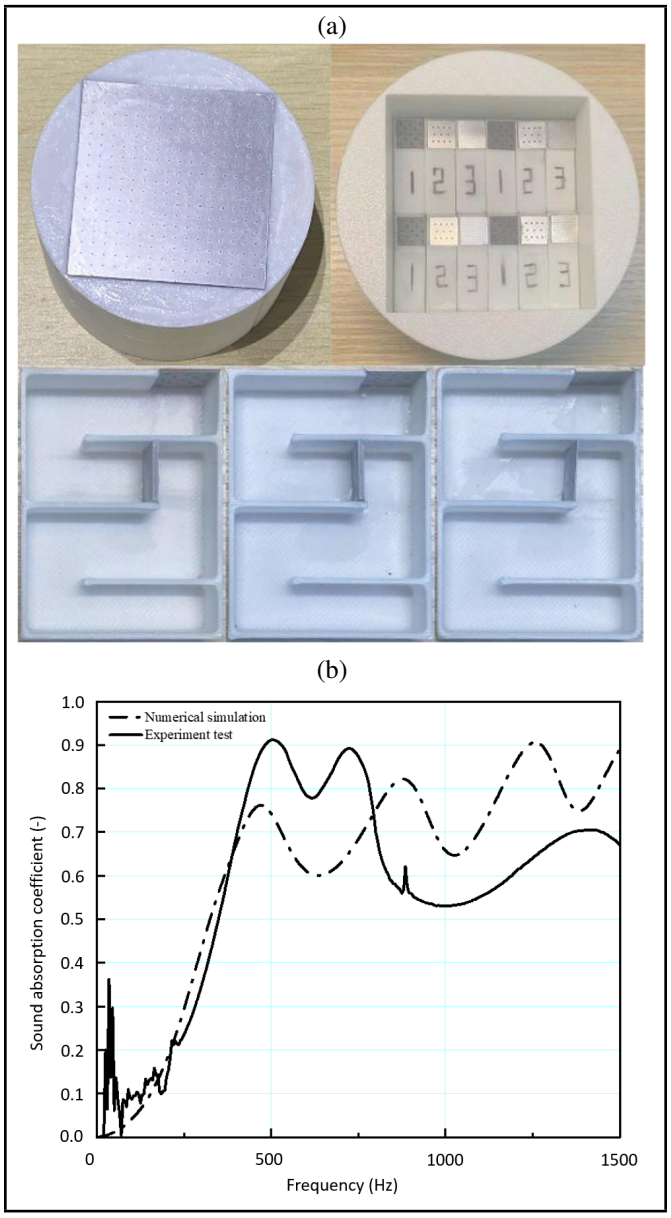

Figure 12. Result of experiment and simulation (a) Sample (b) Sound absorption coefficient.

Electromagnetic Interference Shielding Performance. *Composites Science and Technology*, **195**, 108195, (2020). https://doi.org/10.1016/j.compscitech.2020.108195

[3] Ma, L.F., Yang, W., Wang, Y.S., Chen, H., Xing, Y.F. and Wang, J.C. Multi-Dimensional Strain Sensor Based on Carbon Nanotube Film with Aligned Conductive Networks. *Composites Science and Technology*, **165**, 190–97, (2018). https://doi.org/10.1016/j.compscitech.2018.06.030

[4] Wang, X.T., Wang, B., Wen, Z. H. and Ma, L.F. Fabrication and mechanical properties of CFRP composite three-dimensional double-arrow-head auxetic structures, *Composites Science and Technology*, **164**, 92–102, (2018). https://doi.org/10.1016/j.compscitech.2018.05.014

[5] Ma, L.F., Hu, J.J. and Dou, R. Multiwalled carbon nanotubes filled thermoplastic vulcanizate dielectric elastomer with excellent resilience properties via inhibiting MWCNT network formation, *Journal of Applied Polymer Science*, **138**, 50129, (2021). https://doi.org/10.1002/app.50129

[6] Jiang, C. and Ma, L.F. Polyamide 6-based thermoplastic vulcanizate for thermostability: An experimental and theoretical investigation, *Journal of Applied Polymer Science*, **139**, 51718, (2022). https://doi.org/10.1002/app.51718

[7] Ma, L.F., Liu, C.C., Dou, R. and Yin, B. Significantly improved high dielectric MWCNTs filled PVDF/PS/HDPE composites via constructing double bi-continuous structure, *Composites Part B: Engineering*, **224**, 109158, (2021). https://doi.org/10.1016/j.compositesb.2021.109158

[8] Xu, X.H., Ma, L.F. and Liu, C.C. Bio-based polylactic acid or epoxy natural rubber thermoplastic vulcanizates with dual interfacial compatibilization networks, *Polymer Engineering and Science*, **62**, 1987-1998, (2022). https://doi.org/10.1002/pen.25981

[9] Maa, D.Y. Theory and design of microperforated panel sound-absorbing constructions, *Science in China, Ser. A*, 38-50, (1975).

[10] Maa, D.Y. Design of Microperforated Plate Structure, *Journal of Acoustics*, **13**, 174-180, (1988). https://doi.org/10.15949/j.cnki.0371-0025.1988.03.003

[11] Maa, D.Y. Composite Microperforated Panel Sound Absorbing Structure, *Noise and vibration control*, 3-9, (1990).

[12] Wang, C.Q. and Huang, L.X. On the acoustic properties of parallel arrangement of multiple micro-perforated panel absorbers with different cavity depths, *Journal of the Acoustical Society of America*, **130**, 208-218, (2011). https://doi.org/10.1121/1.3596459

[13] Yang, W.D., Xia, H. and Ni, Q.Q. A double cavity resonant device embedded with porous material and microperforated panel. *Applied Acoustics*, **206**, 109304, (2023). https://doi.org/10.1016/j.apacoust.2023.109304

[14] Li, H.M., Wu, J.W., Yang, S.L. and Mao, Q.B. Design and study of broadband sound absorbers with partition based on micro-perforated panel and Helmholtz resonator, *Applied Acoustics*, **205**, 109262, (2023). https://doi.org/10.1016/j.apacoust.2023.109262

[15] Qian, Y.J., Zhang, J., Sun, N., Kong, D.Y. and Zhang, X.X. Pilot study on wideband absorber obtained by adopting aserial-parallel coupling manner, *Applied Acoustics*, **124**, 48-51, (2017). https://doi.org/10.1016/j.apacoust.2017.03.021

[16] Cobo, H., Jacobsen, F. and Ruzi, H. Optimization of multiple-layer Microperforated panels by simulated Annealing. *Applied Acoustics*, **72**, 772-776, (2011). https://doi.org/10.1016/j.apacoust.2011.04.010

[17] Bucciarelli, F., Malfense Fierro, G.P. and Meo, M. A multilayer microperforated panel prototype for broadband sound absorption at low frequencies. *Applied Acoustics*, **146**, 134-144, (2018). https://doi.org/10.1016/j.apacoust.2018.11.014

[18] Yang, X.C., Bai, P.F., Shen, X.M., To, S. Chen, L., Zhang, X.N. and Yin, Q. Optimal design and experimental validation of sound absorbing multi-layer micro-perforated panel with constraint conditions. *Applied Acoustics*, **146**, 334-344, (2018). https://doi.org/10.1016/j.apacoust.2018.11.032

[19] Wang, X.T., Ma, L.F., Wang, Y.S. and Guo, H. Design of multilayer sound-absorbing composites with excellent sound absorption properties at medium and low frequency via constructing variable-section cavities. *Composite Structures*, **266**, 113798, (2021). https://doi.org/10.1016/j.compstruct.2021.113798

[20] Peng, X., Qiu, C. Li, J.Q., Wu, H.P. Liu, Z.Y. and Jiang, S.F. Multiple-scale uncertainty optimization design of hybrid composite structures based on neural network and genetic algorithm, *Composite Structures*, **262**, 113371, (2020). https://doi.org/10.1016/j.compstruct.2020.113371

[21] Pei, H.B. Structural Parameter Design of Micro-perforated Plate Based on Deep Learning, Hunan University, (2021). https://doi.org/10.27135/d.cnki.ghudu.2021.002379

[22] Li, Y., Liang, B., Tao, X., Zhu, X.F., Zhou, X.Y. and Cheng, J.C. Acoustic focusing by coiling up space. *Applied Physics Letters*, **101**, 233508, (2012). https://doi.org/10.1063/1.4769984

[23] Li, Y., Badreddine M, A. Acoustic metasurface-based perfect absorber with deep subwavelength thickness, *Applied Physics Letters*, **108**, 063502, (2016). https://doi.org/10.1063/1.4941338

[24] Almeida, G. d. N, Vergara, E. F, Barbosa, L. R., Brum, R. Low-frequency sound absorption of a metamaterial with symmetrical-coiled-up spaces, *Applied Acoustics*, **172**, 107593, (2021). https://doi.org/10.1016/j.apacoust.2020.107593

[25] Jiménez, N., Huang, W., Romero-García, V., Pagneux, V. and Groby, J. P. Ultra-thin metamaterial for perfect and quasi-omnidiextional sound absorption, *Applied Physics Letters*, **109**, 121902, (2016). https://doi.org/10.1063/1.4962328

[26] Long, H.Y., Cheng, Y., Tao, J.C. and Liu, X.J. Perfect absorption of low-frequency sound waves by critically coupled subwavelength resonant system, *Applied Physics Letters*, **110**, 023502, (2017). https://doi.org/10.1063/1.4973925

[27] Liu, C.R., Wu, J.H., Chen, X. and Ma, F. A thin low-frequency broadband metasurface with multiorder sound absorption, *Journal of Physics D: Applied Physics*, **52**, 105302, (2019). https://doi.org/10.1088/1361-6463/aafaa3

[28] Tang, Y.F. Ren, S.W., Han, M., Xin, F.X., Huang, L.X., Chen, T.N., Zhang, C.Z. and Lu, T.J. Hybrid acoustic metamaterial as super absorber for broadband low-frequency sound, *Scientific Reports*, **7**, 43340, (2017). https://doi.org/10.1038/srep43340

[29] Jia, X., Li, Y., Zhou, Y.H., Hong, M.H. and Yan, M. Wide bandwidth acoustic transmission via coiled-up metamaterial with impedance matching layers, *Science China Physics*, **62**, 37-44, (2019). https://doi.org/10.1007/s11433-018-9365-6

[30] Xiao, Y., Yu, D.L., Zhao, H.G., Wang, Y., Wen, J.H., and Wu, F. Low-frequency sound absorption of hybrid absorber based on micro-perforated panel and coiled-up channels, *Applied Physics Letters*, **114**, 151901, (2019). https://doi.org/10.1063/1.5090355

[31] Pieren, R. and Heutschi, K. Modelling parallel assemblies of porous material using the equivalent circuit method (Article), *Journal of the Acoustical Society of America*, **137**, EL131-EL136, (2015). https://doi.org/10.1121/1.4905890

[32] Cobo, P., Carlos, dela. C. and Francisco, S. On the modeling of microslit panel absorbers, *Applied Acoustics*, **159**, 107118, (2020). https://doi.org/10.1016/j.apacoust.2019.107118

[33] Liu G.T. and Ji, X.M. A study of characteristics of automobile multilayer soundabsorption material based on transfer matrix, *China Mechanical Engineering*, **25**, 134-137, (2014). https://doi.org/10.3969/j.issn.1004-132X.2004.01.025

[34] Chen W., Lu, C.H., Liu, Z.E. and Du, S.Z. Simplified method of simulating double-layer micro-perforated panel structure, *Automotive Innovation*, **1**, 374-380, (2018). https://doi.org/10.1007/s42154-018-0040-x

[35] Liu, G.T., Ji, X.M. Method for Calculating Sound Absorption Coefficient of the Sound Absorbing Material in the Automobile Cab, *China Mechanical Engineering*, **50**, 104-109, (2014). https://doi.org/10.3901/JME.2014.12.104

[36] Bidi, N. and Elberrichi. Z. Feature selection for text classification using genetical gorithms, *Identification and Control*, 806-810, (2016). https://doi.org/10.1109/ICMIC.2016.7804223

[37] Hassan, M. and Hamada, M. Genetic algorithm approaches for improving prediction accuracy of multi-criteria recommender systems (Article), *International Journal of Computational Intelligence Systems*, **11**, 146-162, (2018). https://doi.org/10.2991/ijcis.11.1.12

[38] Biswas, T., Kuila, P. and Ray, A.K. A novel scheduling with multi-criteria for high-performance computing systems: an improved genetic algorithm-based approach, *Engineering with Computer*s, **35**, 1475-1490, (2019). https://doi.org/10.1007/s00366-018-0676-5

[39] Wang, Y.H., Liu, S.F., Wu, H.Q., Zhang, C.C., Xu, J.K. and Yu, H.D. On-demand optimize design of sound-absorbing porous material based on multi-population genetic algorithm, *E-Polymers*, **20**, 122–32, (2020). https://doi.org/10.1515/epoly-2020-0014

[40] Meng, H., Xin, F.X. and Lu, T.J. Sound Absorption Optimization of Graded Semi-Open Cellular Metals by Adopting the Genetic Algorithm Method, *Journal of Vibration and Acoustics-transactions of the ASME*, **136**, 1-8, (2014). https://doi.org/10.1115/1.4028377